3.9 WP 3.1 Set-up and test of passive MW rain algorithms

Start date or starting event:	**KO**		
Duration	**0-36**		
Participant codes :	**P1**	**P4**	**P6**

Responsible: Partner 6 (Dipl. Met. Martina Kästner, DLR-DFD)

3.9.1 Objectives

- Implementation and evaluation of passive MW precipitation algorithms directly linked to the 3-D structure of the precipitating system using measurements from different sensors like SSM/I on DMSP and TMI/PR on TRMM, based on the data sets collected in WP1.1 with additional cloud physical information from WP2.1 and WP2.2.
- Statistical generation of a cloud-genera oriented radiative data set.
- Development of a MW statistical retrieval algorithm for rainfall parameter estimation.
- Since passive MW techniques perform much better over the oceans than over land comparison with independent information is essential for those areas. The validation of the results obtained is restricted to scientific (TRMM GV sites) and operational (national networks and CERAD) weather radar data. The additional use of airborne radar data is of great value for high-resolution techniques, but is limited for passive MW techniques due to its insufficient spatial coverage.
- In this very early stage great attention has to be kept on the transitivity of the derived results to the common grid (see WP1.3) used in further project WPs such as WP3.3, WP4.1, WP5.1 and WP5.2.

3.9.2 Methodology and scientific achievements

The Algerian severe weather event is used as a common cooperative case study of several partners. The area extends from 15W to 20E and 30 to 60 N and the period is 08 to 13 November 2001. All data are resampled to the common 0.25° lat-lon grid (~28 km). TRMM and InfraRed Estimator (IRE) data do not consistently cover the whole area and the comparison is then conducted over the available part within the common area. The temporal coincidence is optimal for the different PMW algorithms, because PATER and FDA have the same TRMM data base, otherwise the temporal window is better than +/-15 min in the case of the IR (NRL, IRE) and in most cases better than +/-90 min for comparisons with the independent model data, which have a 3-hourly temporal resolution. Comparisons are made for single orbits as well as for merged data within 3-h periods.

The applied rain retrievals are shortly described in the following:
Partner 1: The BOLAM (Bologna Limited Area Model) is a hydrostatic, primitive equation, gridpoint model in σ coordinates, using horizontal wind components, potential temperature, specific humidity and surface pressure as basic dependent variables. The initial and boundary conditions are obtained from the ECMWF 6-hourly analyses.
Partner 1: The basic strategy for the NRL (Naval Research Laboratory) blended technique (Turk et al., 2000) draws upon the probability matching methods developed in the radar meteorology field for specific 'tuned' Z-R relations. Time- and space-coincident IR and MW pixels are collected from different satellites and used to produce dynamically-updated T_B-R lookup tables.
Partner 2: Neural Rain Estimator (NRE) is an operational rapid update IR-based algorithm to diagnose the half-hourly near surface rainfall. It is an empirical technique suited for acquisitions from geostationary satellites. It uses some relevant features of the cloud top evolution and structure and information from NWP model.
Partner 6: The over-ocean PATER is a physical algorithm that uses 2 Empirical Orthogonal Functions (EOF) instead of 9 T_Bs as a rain rate predictor. The retrieval database is generated from several cloud model simulations described in Bauer (2001). The algorithm set-up (Bauer et al., 2001) has a stand-alone PMW component and is optionally calibrated by carefully co-located PR estimates. Currently it is foreseen for an operational implementation into the ECMWF assimilation scheme.
Partner 7: The frequency difference algorithm (FDA) by Ch. Kidd is a pure PMW satellite rain algorithm that is operationally applied to TRMM and SSM/I orbit data.

The results of the inter-comparison of different rain retrievals are given for visual inspection at the same fixed date (10 Nov 2001, 0300 UTC) (Fig. 3.37-3.41). A complete analysis of the categorical statistics of all possible dates within the period 08 to 13 Nov 2001 is then given in Table 3.3.

Based on the analysis each with two techniques in the inter-comparison, **Partner 6** assesses both PMW algorithms, PATER and FDA, of similar quality to retrieve rainfall regions and intensities (Fig. 3.37 and 3.38). There are three areas of heavy rainfall, one west of the Canary Islands, the biggest one around Algiers, and the last southeast of Sardinia. The three rain areas coincide in raifall products from both MW algorithms very well. Even the rain intensities are similar except for the Sardinia

area. The FDA works over land and ocean, the PATER exclusively over ocean and for rainfall rates above 1 mm h^{-1}. The low rain rates smoothly distributed over the sea south of Sicily (Fig. 3.37) are erroneously assigned rain while the area is covered by a strong desert aerosol transport that fell out over Rome the next day. The rainy speckles over the Atlantic are due to cumulus convective showers within the cold air. Compared to the PMW techniques the BOLAM model rainfall (before nudging) shows wide agreement of the rain bands (Fig. 3.39). The rainfall intensities were rather similar, only the position of the rainfall had a location error for the Sardinia area. The two IR-based algorithms, NRL and IRE (Fig. 3.40 and 3.41) give strong rain areas over the Mediterranean Sea, but not at the correct position. The Algerian coast, where the maximum precipitation fell, is hardly classified as a heavy rain area. The combined MW/IR NRL algorithm had a much better performance than the pure IR algorithm IRE.

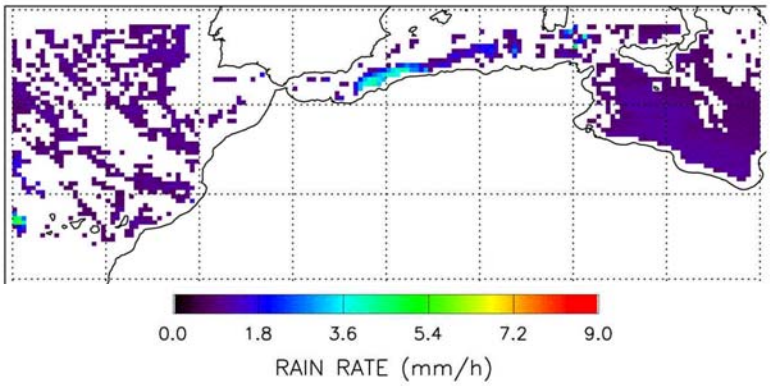

Figure 3.37. PATER rain retrieval, 10 November 2001, orbit 22741+22742, 0025+0203 UTC – MW.

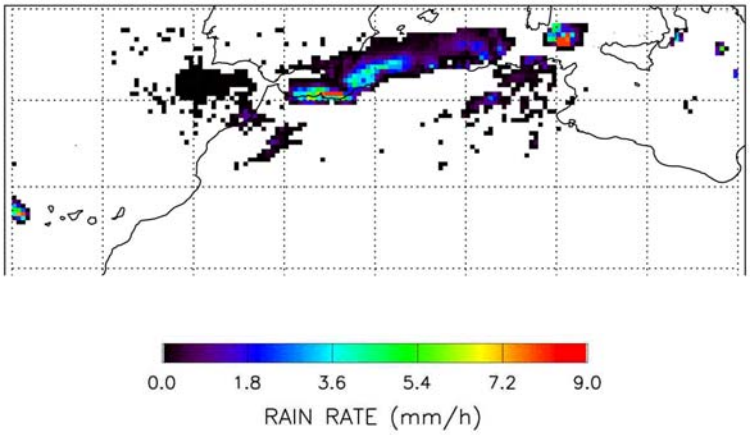

Figure 3.38. Same as in Fig. 3.37, but for FDA (frequency difference algorithm) – PMW.

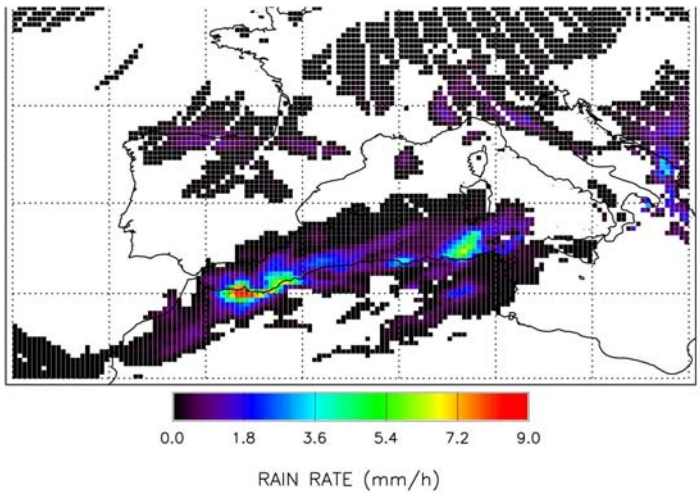

Figure 3.39. BOLAM, 10 November 2001, 0300 UTC – model.

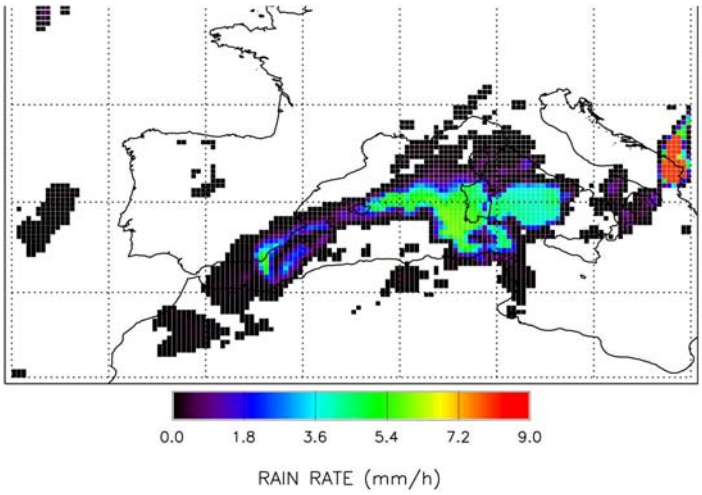

Figure 3.40. NRL algorithm, 10 November 2001, 0300 UTC – combined IR-MW.

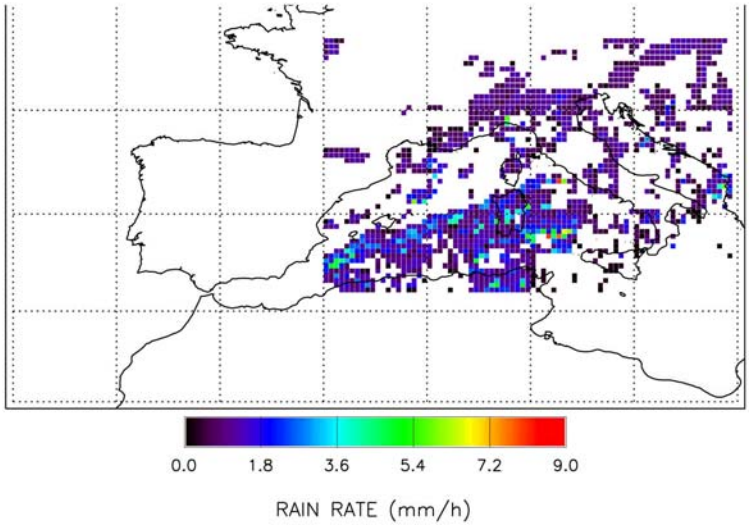

Figure 3.41. IRE, 10 November 2001, 0300 UTC – IR.

Overall it seems to be favourable to combine the high temporal resolution of IR with the better performance of rainfall identification of MW techniques for monitoring purposes. The NRL algorithm or the TRMM 3B42 products belong to this category. The low MW pixel resolution makes a 0.25° lat-lon grid appropriate, but better spatial resolution is desired by the users.

The event occurrences of the contingency table for comparisons within the time period 09 to 11 Nov 2001 regard the above mentioned temporal windows (Table 3.3). The number of compared pairs N differs for each algorithm pair, thus, the occurrences are given in percent of N for better comparison between the cases, the maxima (e.g. hits) or minima (e.g. false alarms) are italicized, respectively.

The accuracy of all inter-comparisons is measured in terms of Heidke skill score, ranging from 0.61 (BOLAM vs. NRE) to a respectable 0.76 (BOLAM vs. NRL). No bias between the data sets is indicated when the bias value is unity, thus, PATER and NRL have only a small bias. Note, that even in this heavy rain event only 10% of the gridded pixels are hits (rain/rain), whereas the correct negatives (no-rain/no-rain) appear to nearly to a factor of 7 of that (62%).

	Compared pairs	hits	misses	false alarms	correct negatives	Heidke skill score (accuracy)	Bias score
	N = 100%	%	%	%	%	best = 1	best =1
PATER vs. BOLAM	8.346	4.9	21.1	11.9	62.2	0.67	0.65
PATER vs. NRE	2.595	7.2	16.6	20.0	56.1	0.63	1.14
PATER vs. NRL	14.619	3.3	14.3	15.2	67.2	0.70	1.05
BOLAM vs. NRE	3.774	22.3	10.0	28.6	39.2	0.61	1.58
BOLAM vs. NRL	13.880	9.9	13.3	10.9	65.9	0.76	0.89
NRE vs. NRL	6.320	20.6	15.6	11.1	52.6	0.73	0.88
FDA vs. PATER	3.353	2.5	8.9	8.9	79.7	0.82	1.01
FDA vs. BOLAM	6.128	11.2	18.3	4.2	66.3	0.78	0.52
FDA vs. NRL	7.142	5.0	15.2	3.9	75.9	0.81	0.44
FDA vs. NRE	931	12.5	23.3	7.8	56.3	0.69	0.57
TOTAL	67.088	9.9	15.7	12.3	62.1	0.72	0.87

Table 3.3. Categorical statistics of different satellite rain retrievals.

For the selected meteorological situation with heavy rainfall throughout the day the validation study elucidated some problems. The maximum rain rate was smoothed down to a factor of 2 by resampling from TRMM orbit to gridded data. Further, the correlation coefficient of two data sets is dependent on the grid resolution and the rain/no-rain threshold. The statistics are ruled by the correct negatives and not by the hits. It may well be that the use of entity-based methods, like the CRA (contiguous rain area), verification gives further insight into the algorithm performances (Ebert 2000). Misses and false alarms are usually higher than the hit rate, this indicates the need of further refinement of the analysed techniques.

The study shows that reasonable precipitation areas may be received from TRMM using a combination of active and passive MW data as the PATER algorithm. The retrieval is crucially dependent on the forward 3-D cloud model calculations and there is a need for improved cloud models that cover the whole spectrum of natural clouds. In this case study both the PMW techniques performed better than IR techniques. A combination of PMW and IR is recommended that combines the possibilities of a better rain detection with a better temporal resolution.

3.9.3 Tests of GPROF v5 and v 6 algorithms

Partner 1 has conducted studies on the ability of the Goddard Profiling (GPROF) (Kummerow et al. 2001) algorithm in gauging rain over land. GPROF version 5 and 6 were installed. Note that GPROF5 and 6 for now work on data from the TMI and v6 is being adapted to the SSM/I. After careful comparison of GPROF5 rain rate estimates with ground validation data, GPROF6 has been tailored for a better matching of precipitation radar and ground observations. Moreover, it includes an improved classification of stratiform–convective precipitation. On a global scale, GPROF6 eliminates the high bias with respect to gauges. The space-time coincident PR measurements allow for a direct comparison of rainfall data derived from PMW (TMI radiometer) with reference data.

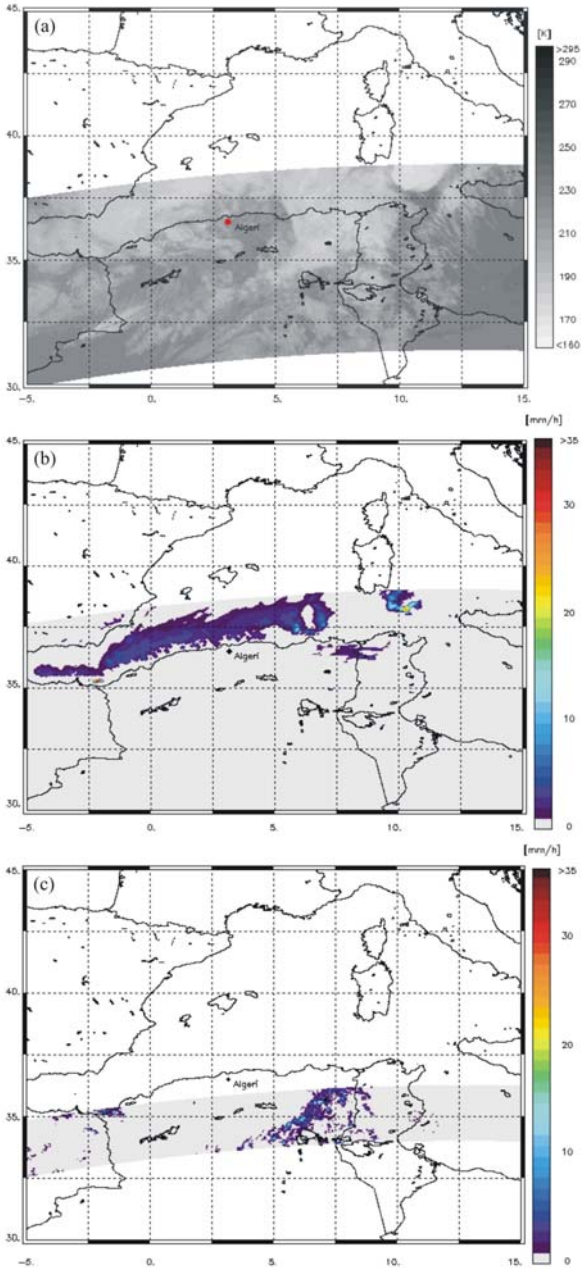

Figure 3.42. TRMM 22741 overpass: (a) IR T_B from 1B01 TRMM product; (b) GPROF surface rainrate from 1B11 product; (c) PR-derived surface rainrate from 2A25 product.

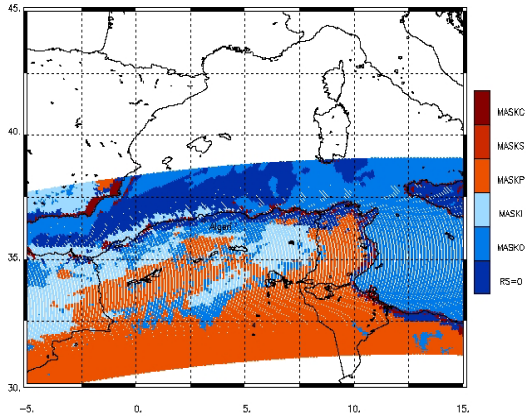

Figure 3.43. Results of the masking procedure of GPROF6 on the 22741 overpass. Pixel identified by RS=0 are being retained for the retrieval.

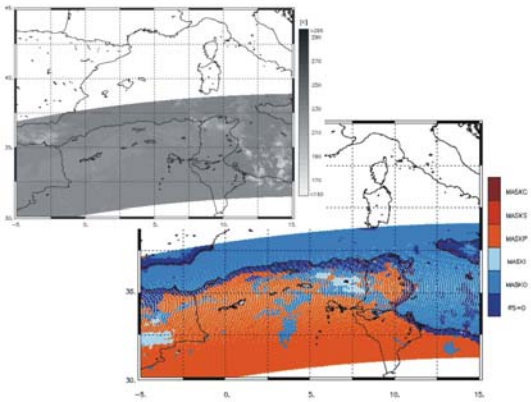

Figure 3.44. IR VIRS image and screening results from the TRMM overpass 22634 on 3 November 2001 0345 UTC.

Figure 3.45. MODIS multispectral image of Algeria on 28 April 2002.

The Algerian flood served as a testbed for verifying the performances of the pixel screening and the convective-stratiform assignement over land and ocean. The difficulty of the case as a coastal rain event is ideal in this perspective. Two TRMM overpasses on 10 November 2001 were studied: the 22741 ascending orbit passing over Algiers at 0032 UTC and the 22742 descending orbit that passed at 0209 UTC. Fig. 3.42 shows the IR T_B, the GPROF 1B11 surface rainrate and the PR 1A25 rainrate for the 22741 overpass. Note the relatively poor performance of GPROF6 over land and along the coast with respect to the PR product. This fact can be attributed to the scarce number of profiles over land (only 135 with respect to 12068 over the ocean). Secondly, there is no specific database available for coastal areas. Finally, there are possible errors in the pixel screening procedure that prevent the correct delineation of rainy areas. In fact a large number of pixels is screened out over land and along the coast due to the masking procedure (Fig. 3.43).

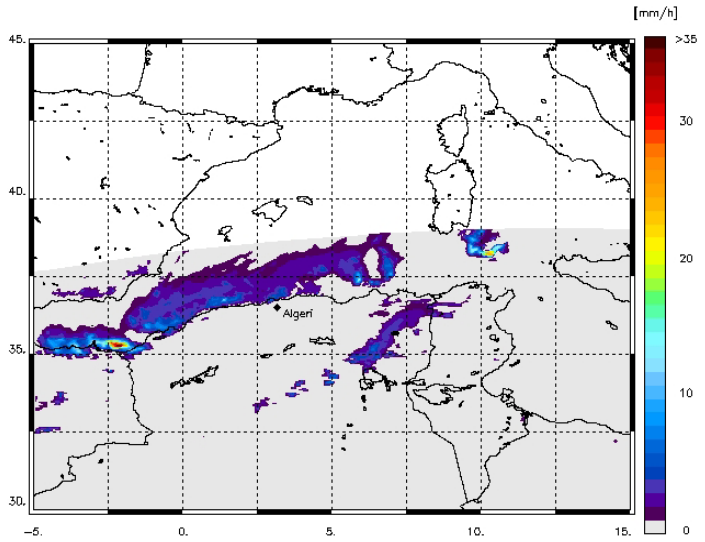

Figure 3.46. Rainrate estimate using GPROF6 for the 22741 computed by modifying the screening procedure.

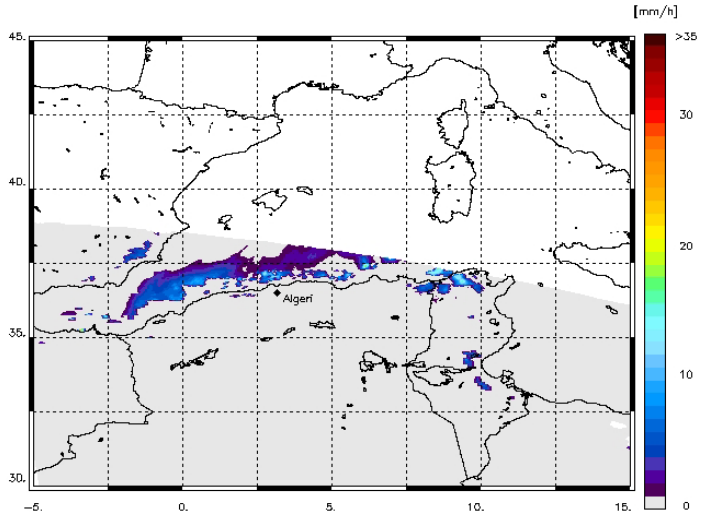

Figure 3.47. Surface rainrate for the 22742 overpass from the 2A12 GPROF5 product.

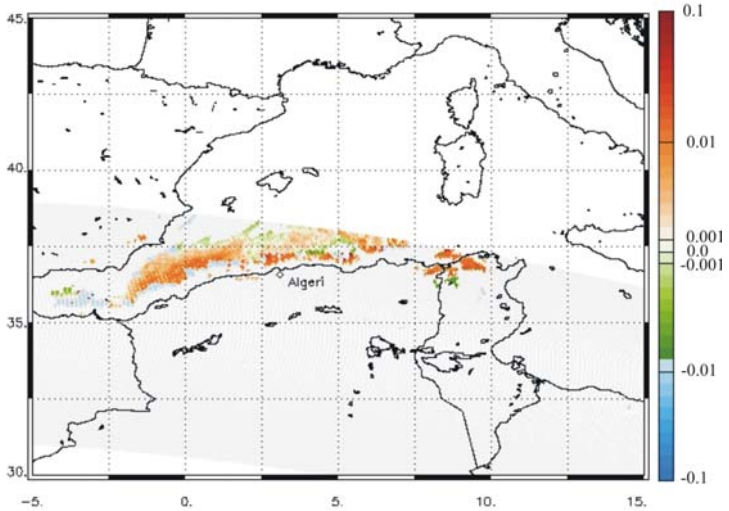

Figure 3.48. Percent relative difference between surface rainrates from GPROF6 and GPROF5 for the 22742 overpass.

By comparing the screening results with the overpass 22634 on 3 November 2001 (Fig. 3.44) (selected because of a cloud free situation and its closeness to the 22741 time) the generally good performance of the screening is proved in terms of the tests applied over the coast. Several pixels are cancelled over land attributed to ice or non precipitating clouds. The problem, however, is that nearly the totality of land pixels is eliminated due to the high polarization. This is more or less always the case as it results from the analysis of other passages. Fig. 3.45 shows northern Algeria in cloud free conditions as seen from MODIS multispectral imagery. Two mountain chains are visible, the Tell Atlas and the Saharan Atlas that encircle semi-arid high plains that are interrupted by depressions (*chott*) displayed in gray. The Saharan Atlas delimits the desert area in the north.

It is possible to match surface rainrates from PR and TMI by modifying those screening procedures that involve the presence of ice over land and coast (Fig. 3.46). Inspite of these corrections, however, precipitation went undetected over Algier: measurements are confined along the coast and never come inland. This demonstrates that not only a larger database is necessary but also screenings need to be adapted to the surface characteristics of the area. This shows the necessity of applying these global algorithms locally in order to test their performances in view of operational applications.

An image of the GPROF 5 rainrate for the 22742 overpass is shown in Fig. 3.47. There are no substantial differences between the two products although improvements should have happened over land due to the different convective-stratiform separation in GPROF6. In order to quantify the differences between the two products the percent relative difference was computed as follows

$$diff = \frac{(sfcrainV5 - sfcrainV6)}{sfcrainV6} \Big/ 100$$

where 5 and 6 refer to the two versions. Results are shown in Fig. 3.48 where positive values indicate an underestimate of GPROF6 with respect to GPROF5 and viceversa. Abrupt sign changes are due to the different computed precipitation type. This is confirmed by the PR convective-stratiform separation from the radar product (Fig. 3.49). Unfortunately only a small portion of the TMI precipitation area is covered by the PR but in the stratiform region GPROF6 is shown to be underestimating and the opposite within the convective area.

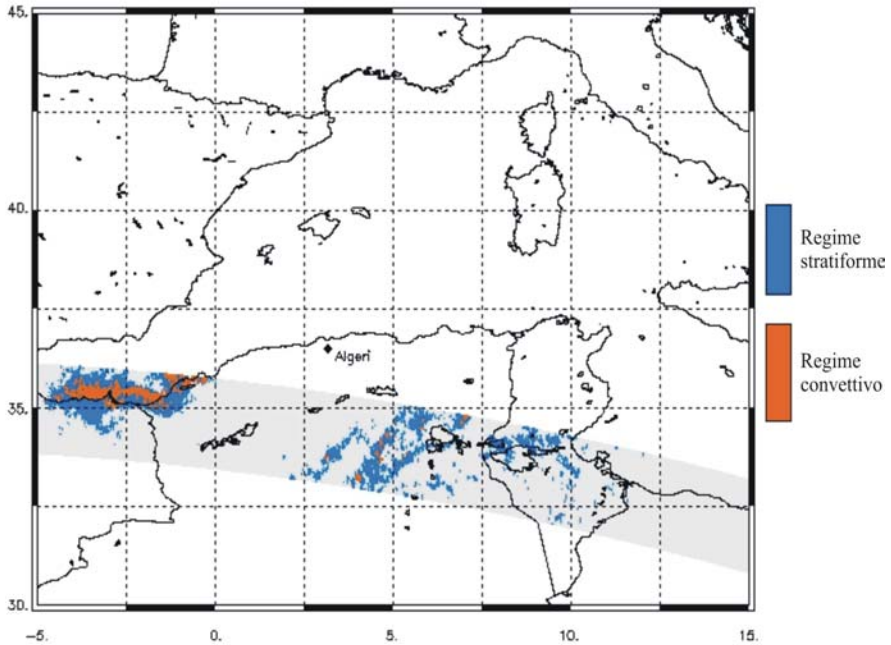

Figure 3.49. Convective-stratiform discrimination from the PR products for the 22742 overpass.

3.9.4 References:

Bauer, P., 2001: Over–ocean rainfall retrieval from multisensor data of the Tropical Rainfall Measuring Mission. Part I: Design and evaluation of inversion databases. *J. Atmos. Oceanic Technol*., **18,** 1315-1330.

Bauer, P., P. Amayenc, C. D. Kummerow, and E. A. Smith, 2001: Over–ocean rainfall retrieval from multisensor data of the Tropical Rainfall Measuring Mission. Part II: Algorithm implementation. *J. Atmos. Oceanic Technol*., **18,** 1838-1855.

Bolle, H.-J. (Ed.), 2003: *Mediterranean Climate – Variability and Trends*. Springer, Berlin, 372 pp.

Ebert, E. E., and M. J. Manton, 1998: Performance of satellite rainfall estimation algorithms during TOGA COARE. *J. Atmos. Sci*., **55,** 1537-1557.

Ebert, E. E. and J. L. McBride, 2000: Verification of precipitation in weather systems: determination of systematic errors. *J. Hydrol*., **239,** 179-202.

Kummerow, C. D., Y. Hong, W. S. Olson, S. Yang, R. F. Adler, J. McCollum, R. Ferraro, G. Petty, and T. T. Wilheit, 2001: The evolution of the Goddard Profiling Algorithm (GPROF) for rainfall estimation from passive microwave sensors. *J. Appl. Meteor.*, **40**, 1801-1820.

Turk, J. F., G. Rohaly, J. Hawkins, E. A. Smith, F. S. Marzano, A. Mugnai, and V. Levizzani, 2000: Meteorological applications of precipitation estimation from combined SSM/I, TRMM and geostationary satellite data. In: *Microwave Radiometry and Remote Sensing of the Earth's Surface and Atmosphere*, P. Pampaloni and S. Paloscia Eds., VSP Int. Sci. Publisher, Utrecht (The Netherlands), 353-363.